 CMC, vol.43, no.3, pp.137-151, 2014

Modeling of Hydro-Viscoelastic State of Deformable and Saturated Product During Convective Drying

R. Lamloumi[1,2], L. Hassini[1], G. L. Lecomte-Nana[2], M. A. Elcafsi[1] and D. Smith[2]

Abstract: A mathematical model was developed to simulate in 2D the spatio-temporal evolution of the moisture content, the temperature and the mechanical stress within a deformable and saturated product during convective drying. A comprehensive hydro-thermal model had been merged with a Maxwell model with two branches, assuming a viscoelastic material, a plane deformation and an isotropic hydric-shrinkage of the sample. A long sample of clay mixture with a square section was chosen as an application case. The transport and equilibrium properties of the product required for the modeling were determined from previous experiments which were independent of the drying trials. In order to validate the hydro-thermal part of the model, several drying tests were carried out for different values of temperature, relative humidity and air velocity in a vertical drying tunnel (designed and constructed in the LETTM laboratory). The theoretical and experimental results appeared in good agreement. The simulations of the spatio-temporal distribution of mechanical stress were performed and interpreted in terms of product potential damage. The sample shape was also predicted all aver the drying process with reasonable accuracy.

Keywords: hot-air convective drying, modeling, viscoelastic stress, clay mixture, cracking risk.

Nomenclature

C_p	specific heat capacity	$Jkg^{-1}K^{-1}$
D	hydric diffusivity m	$^2s^{-1}$
E(t)	relaxation function	MPa

[1] Université de Tunis El Manar, Tunisie ; Faculté des Sciences de Tunis, laboratoire d'Energétique et des Transferts Thermique et Massique (LETTM).

[2] Université de Limoges, France; Ecole Nationale Supérieure de Céramique Industrielle (ENSCI), laboratoire Groupe d'Etude des Matériaux Hétérogènes (GEMH).

G(t)	Shear modulus	MPa
K(t)	Bulk modulus	MPa
RH	air relative humidity	%
t	time	s
T	temperature	$^{\circ}$C
v	velocity	ms^{-1}
V	volume	m^3
X	water content (db)	$kgkg^{-1}$

Greek letters

α	linear hydro-contraction coefficient (wb)	
β	volumetric hydro-contraction coefficient (db)	
δ_{ij}	Kronecker's delta	
ε_{ij}	total strain tensor	
λ	thermal conductivity	$Wm^{-1}K^{-1}$
ν	Poisson's ratio	
ρ	density	kgm^3
σ_{ij}	stress tensor	Pa

Subscripts

0	initial
a	air
l	liquid
s	solid

1 Introduction

The speeding up of industrial drying processes by applying enhanced operating conditions is often limited by the occurrence of cracks in the skin of the product. The cracks may lead to a global failure (ceramics) or simply alter the visual aspect of the product (pasta, vegetables). In order to avoid these defects, the very complex influence of the drying conditions on the internal stresses and deformations of a product during the process must be assessed.

In recent years different mechanical models have been proposed to describe the stresses within the product during the drying. Several drying models consider an elastic behavior [Jomaa and Puiggali (1991); Arrieche, Corrêa and Sartori (2009)].

However, the elastic theory is not acceptable for products witch possess the capacity to store and dissipate mechanical energy. The viscoelastic theory is more realistic to describe the history effect and foresee correctly the deformation in many wet products subjected to drying, like: clays, ceramics and food products. The Maxwell constitutive equations were commonly used to express viscoelastic properties [Jomaa and Puiggali (1991); Arrieche, Corrêa and Sartori (2009)] [Solomon and Jindal (2007); Qian, Dong, Wang, Özkan and Mao (2010)].

This work is a contribution to the large task of the modeling of mechanical phenomena occurring inside deformable product during drying processes. Its objective was to propose a comprehensive and rigorous 2-D mathematical description of the hydro-thermo-mechanical state of a deformable and water saturated product during convective drying. The model was implemented using the COMSOL Multiphysics finite-elements solver. The coupled heat and mass transfer equations, mechanical equilibrium equations along with the generalized Maxwell's rheological behavior law were solved simultaneously on a variable geometrical domain. In that way and unlike in some other works on this subject, the actual deformation of the sample respecting the global equilibrium and boundary constraints, and not an arbitrary one, was applied to solve the heat and mass balances. A long parallelepipedical sample of clay mixture with a square section was chosen as the study case. In order to implement and validate the model, the hydro-viscoelastic properties and the drying kinetics of the product were measured on the facilities of the LETTM laboratory. Simulations of the temporal evolution of mechanical stress at different specific points of the sample were explored and interpreted in terms of the cracking risk of the product. A comparison between the results obtained by viscoelastic and elastic models was performed. Besides, the sample shape evolution during drying was predicted.

2 Modeling

2.1 Assumptions

• The material consisted of non compressible solid (dry matter) and liquid (water) phases,

• The liquid vaporized only at the surface of the sample,

• The shrinkage was ideal and isotropic,

• The material behaved according to Maxwell model, of viscoelasticity with infinitesimal strain,

• The deformation was plane over the (x,y) plane.

2.2 Heat and mass transfer equations

The heat and mass transfer model consisted on the liquid phase diffusion/advection equation (eq. 1) and the heat diffusion/advection equation (eq. 2). The advective terms due to shrinkage were written using the solid matter velocity (v_s) which was the coupling variable between the hydro-thermal and mechanical equations. This velocity was determined by solving simultaneously the mechanical part of the model. The magnitude of hydric shrinkage was described by means of the volumetric dry basis hydro-contraction coefficient β.

$$\frac{1}{1+\beta X}\frac{\partial X}{\partial t}=\frac{\partial}{\partial x}\left(\frac{D}{1+\beta X}\frac{\partial X}{\partial x}\right)+\frac{\partial}{\partial y}\left(\frac{D}{1+\beta X}\frac{\partial X}{\partial y}\right)-\frac{v_s^x}{1+\beta X}\frac{\partial X}{\partial x}-\frac{v_s^y}{1+\beta X}\frac{\partial X}{\partial y} \tag{1}$$

$$\begin{aligned}&\frac{\rho_s(C_{ps}+XC_{pl})}{1+\beta X}\frac{\partial T}{\partial t}\\&=\frac{\partial}{\partial x}\left(\lambda\frac{\partial T}{\partial x}\right)+\frac{\partial}{\partial y}\left(\lambda\frac{\partial T}{\partial y}\right)-\frac{\rho_s(C_{ps}+XC_{pl})}{1+\beta X}v_s^x\frac{\partial T}{\partial x}-\frac{\rho_s(C_{ps}+XC_{pl})}{1+\beta X}v_s^y\frac{\partial T}{\partial y}\end{aligned} \tag{2}$$

In general, β depend on moisture content and temperature, but in linear theory it will be considered as constant and given by the following expression:

$$\beta=\frac{V-V_s}{XV_s} \tag{3}$$

In the case of isotropic shrinkage, β can be related to the linear wet basis hydro-contraction coefficient α, which is used in the equation 7, as follows:

$$3\alpha=\frac{V_s}{V_0}\beta \tag{4}$$

where V_s is the dry sample volume and V_0 is the initial (fully wet) sample volume. The α value was determined experimentally in our laboratory.

2.3 Structural mechanics equations

The mechanical model consisted mainly on the mechanical equilibrium equation (eq. 4) and the viscoelastic behavior equation (eq. 5) as appeared in Itaya, Okouchi and Mori (2001); Toujani, Djebali, Hassini, Azzouz and Belghith (2014); Mercier (1996).

$$\nabla(\sigma_{ij})=0 \tag{5}$$

$$\sigma_{ij}(t) = \int_0^t (K(t-\tau) - \frac{2}{3}G(t-\tau))\frac{\partial \varepsilon_{ij}^m(\tau)}{\partial \tau}\delta_{ij}d\tau + 2\int_0^t G(t-\tau)\frac{\partial \varepsilon_{ij}^m(\tau)}{\partial \tau}d\tau \quad (6)$$

G and K are shear and bulk modulus, respectively, determined from the following expressions:

$$G(t) = E(t)/3(1-2\nu), \quad K(t) = E(t)/2(1+\nu) \quad (7)$$

E(t) is the relaxation function also called the instantaneous Young modulus and ν is the Poisson's ration. The relaxation expression used here was of the clay witch was determined experimentally by Hammouda and Mihoubi (2013).

The total strain, observed strain ε_{ij}, is a function of changes in mechanical strain ε_{ij}^m (deformation due to viscoelasticity) and in hydric shrinkage strain (deformation proportional to moisture content), as expressed by equation (6):

$$\varepsilon_{ij} = \varepsilon_{ij}^m + \varepsilon_{ij}^h \quad (8)$$

$$\varepsilon_{ij}^h = \alpha\,(X - X_0)\;\delta_{ij} \quad (9)$$

In numerical solid mechanics, these equations are solved not in terms of strain (ε) but in terms of displacements (u) in the x and y directions. The relations between displacement, strain and solid matter velocity are given below.

$$\varepsilon_{ij} = \frac{1}{2}\left(\frac{\partial u_i}{\partial x_j} + \frac{\partial u_j}{\partial x_i}\right), \quad i,j = x,y \quad (10)$$

$$v_s^i = \frac{\partial u_i}{\partial t} \quad (11)$$

The paper claims to deal with deformable product, but the equation 9 postulates small deformation. Indeed, clay mixture sample drying process lasts several hours. The model was written in incremental, that is to say that between two small successive time steps of the numerical resolution, the product can be considered in a small strain state. This explanation was given by Jomaa and Puiggali (1991); Mercier (2005).

2.4 Initial and boundary conditions

• The sample was initially at an uniform temperature and water content and was stress free,

• The heat and water transfer at the sample surface in contact with air was supposed to be purely convective,

• The external sample faces were free of external loading,

• The heat and mass transfer and the displacements at the surface in contact with the shelf were considered nil.

2.5 Model implementation

Because of the symmetry of the problem (see Fig. 1), the above described model was solved on a two-dimensional domain spanning over the half (5mmx10mm) of a cross-section of the potato sample. The governing equations as well as initial and boundary conditions were numerically implemented by means the COMSOL Multiphysics finite-elements software (version 3.3a) using both the 'Chemical Engineering' and the 'Structural mechanics' modules and moving mesh application mode. The computational mesh was defined by means of triangular elements. The direct (UMFPACK) linear system solver was used.

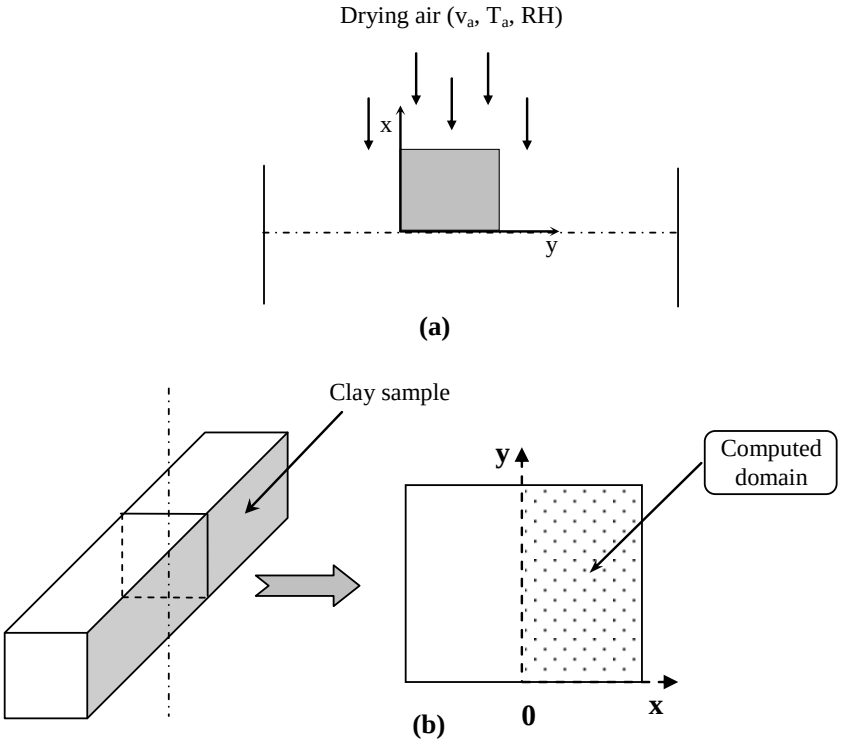

Figure 1: a- The sample orientation in the drying tunnel and b-the computed domain.

3 Results

3.1 Hydro-thermal state simulation

The clay mixture used in this study is a commercial product obtained from BIBLIONTEK Company [Lecomte-Nana, Barre, Nony, Lecomte, and Terracol (2013)]. This mixture contains clay RR32, halloysite, vermiculite, clay 24: Sereilhac clay with moisture content dry basis equal to 35%. One of the important applications of such clay mixture is for the processing of boxes devoted to the preservation of heritage and precious objects against fire damage and other degradation (moisture, insects, etc.).

The clay viscoelastic properties used for the simulation were available in the work of Hammouda and Mihoubi (2013) . In this paper, the relaxation function against testing time was represented by the following Prony series:

$$E(t) = E_c + E_1 \exp(-t/\tau_1) + E_2 \exp(-t/\tau_2) \tag{12}$$

where, E(t) is the elastic modulus at any time, E_1 and E_2 are the elastic modulus for each Maxwell component, τ_1 and τ_2 are relaxation times, and E_c is the equilibrium elastic modulus. The values of these parameters are determined by fitting the experimental relaxation function by equation 11 (Table 1).

Table 1: Values of relaxation parameters.

E_c(MPa)	E_1(MPa)	E_2(MPa)	τ_1(s)	τ_2(s)
0.02	0.22	0.71	37.03	5000

In order to validate the model, drying experiments were carried out for different operating condition: different values of temperature, relative humidity and air velocity (see Fig. 1). A long clay mixture slab with square section (dimensions: 60x10x10 mm) was chosen as a testing material.

The drying tunnel (designed and constructed in the LETTM laboratory, Faculté des Sciences de Tunis) was of vertical type with full control of the drying air parameters (the layout of the dryer is given in a previous paper [Hassini, Azzouz, Peczalski and Belghith (2007)]. Simulations are run for various drying conditions.

The experimental and simulated temporal-evolution of the sample mean moisture content and center point temperature are presented on Fig. 2. Others curves confirmed the model validation were performed but not presented here. There was a good agreement between the experimental and simulated results, especially as

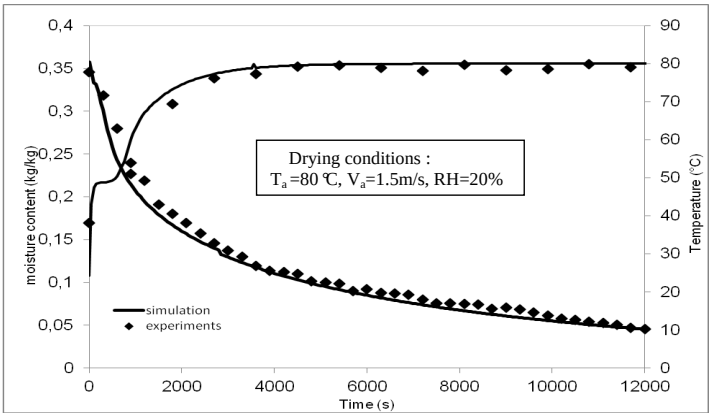

Figure 2: Mean moisture content and center material temperature versus time.

concerns the core temperature. For all drying conditions, the relative difference between the experimental drying time and the simulated one is less than 10 %, which is quite satisfactory. The slight misfit observed could be attributed in one part to measurements errors (especially in the mass record due to the support vibration generated by the airflow and in the temperature record due to the imprecision of thermocouple positioning at the centre of the sample), and in the other part to the simplifying hypothesis of the model (especially ideal isotropic shrinkage).

The sample temperature profile exhibited a small plateau at a value corresponding to the wet-bulb temperature of the hot air witch indicated the existing of a constant drying rate phase in the considered drying process.

The moisture content distributions within the sample after drying times of 900s and 7200s are presented on Fig. 3. For all iso-lines plots in this paper, the external rectangular frame of the plots represents the initial sample contour while the internal curved frame represents the current slab contour. As expected, it could be observed that, at the beginning of the process, the water content gradient was much stronger at the top surface than at the bottom of the sample. At the end of drying, the moisture content became uniform throughout the domain and reached the equilibrium value with the ambient air. It should be noted that a non-uniform distribution of the moisture content during the drying process will generate internal stress and strain what will be analyzed in the next section. The temperature distributions within the sample at drying times of 900s and 7200s are presented on Fig. 4. It could be observed that the temperature inside the sample was practically uniform during all the process, and therefore the internal diffusion of water was the limiting phenomena for water removal for this process.

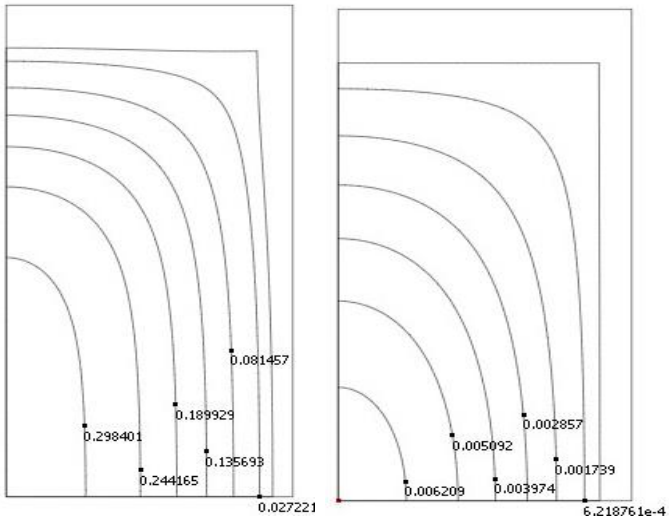

(t = 900s) (t = 7200s)

Figure 3: The moisture content distributions within the sample at 900s and 7200 of drying. (T_a= 80˚C, v_a= 1.5 m/s, RH = 20%)

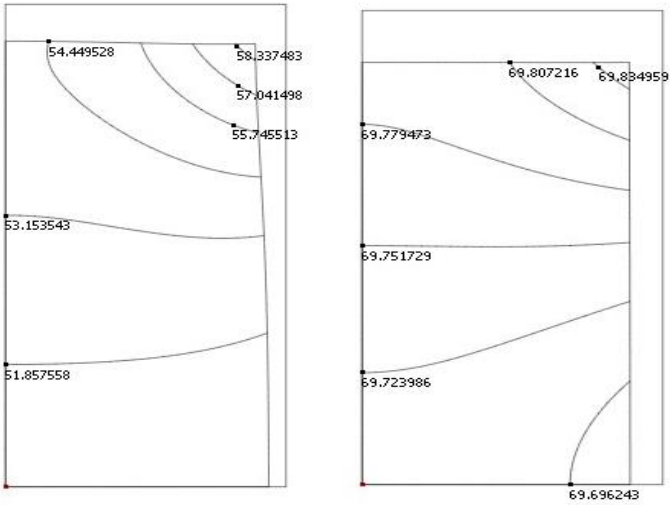

(t=900s) (t=7200s)

Figure 4: The temperature distributions within the sample at 900s and 7200s (T_a = 80˚C, v_a= 1.5 m/s, RH = 20%)

3.2 Mechanical state simulation

The distribution of mechanical stress within the sample at drying times of 900s and 7200s are presented respectively on Figs. 5 and 6 where case (a) depicts the normal stress σ_{xx} in the x direction at 900s, (b) the normal stress σ_{yy} in the y direction and case (c) the shear stress σ_{xy} in the (x,y) plane These profiles, as well as all the others presented later in this paper, were determined for a (x,y) plane at the middle length of the sample. Conventionally, the positive and negative values of the stress correspond to the tensile and compressive stresses, respectively.

According to our results, at the beginning of the drying process (t = 900s) the superficial sample layer (in contact with hot air) was in traction while the core of the sample was in compression, as a consequence of the mechanical equilibrium. At the middle of the process (t = 7200s) the superficial sample layer was in compression and the core of the sample was in traction, indicating that the stress changed its sign during the drying course. At the end of drying, the stress relaxed to zero (Fig. 7). This phenomenon of stress reversal was demonstrated by some authors when a viscoelastic model was adopted [Perré and Passard (2004); Banaszak and Kowalski (2005); Rémond, Passard and Perré (2007); Khalfaoui, Chemkhi and Zagrouba (2013)].

Figure 7 shown that , the stress level raised rapidly at the beginning of drying, (because of the increase of the moisture gradient), passed by a maximum (corresponding to the beginning of the falling rate period) and decreased thereafter to reach a weak second maximum of the opposite sign and then return to zero, when the moisture gradient tended to zero.

According to Fig. 6, the maximum stress was located on the sample face in contact with air. This was due to the high hydric shrinkage in this region and indicated that the risk of cracking affected only this face. However, these cracks, if they existed, could not expand into the inner part of the sample because it was in compression. It is also interesting to note that the normal stress in the x direction at the upper sample surface was lower than the normal stress on the lateral surface, so that the cracks were more likely to appear at the lateral surface of the sample.

Fig. 8 allows us to compare the evolution of elastic and viscoelastic stress with time. Indeed, at the beginning of the process the profiles are similar and reach their maxima at the almost the same time. The values of stress calculated by the viscoelastic model were lower than those obtained by the elastic model. This last result is similar to that found by Kowalski and Rajewska (2002) in the case of a clay cylindrical sample dried convectively. However, Khalfaoui, Chemkhi and Zagrouba (2013) demonstrated that the viscoelastic stress was greater than the elastic stress for a parallelepipedical clay sample.

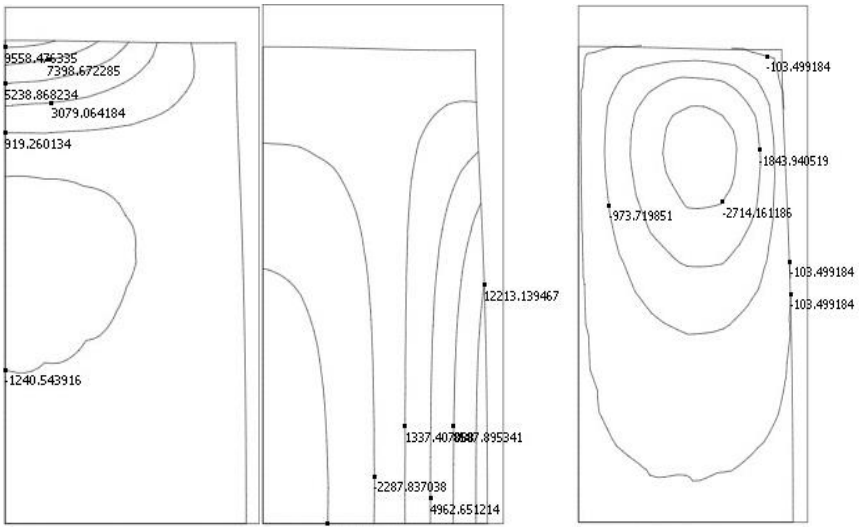

(a) (b) (c)

Figure 5: Normal and Shear stress distribution (a-σ_{xx}, b-σ_{yy}, c-σ_{xy}) at t = 900 of drying. (T_a = 80˚C,v_a= 1.5 m/s, RH = 20%)

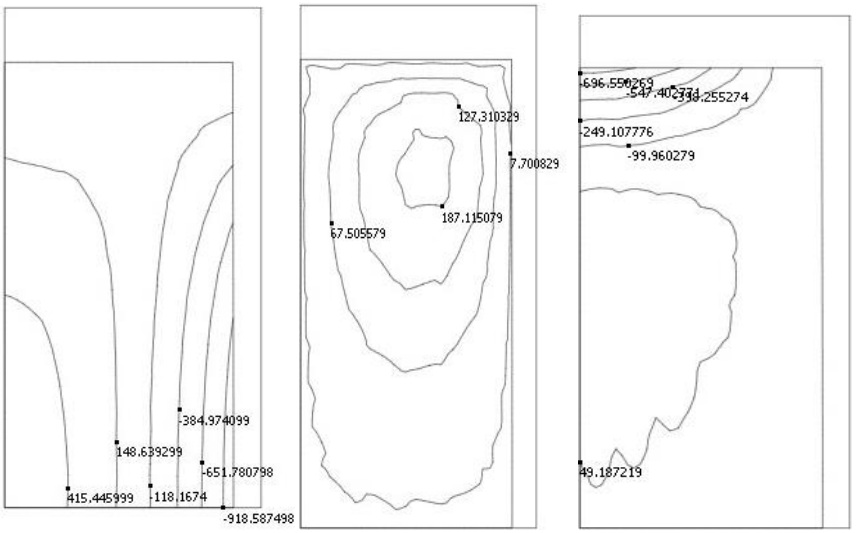

(d) (e) (f)

Figure 6: Normal and Shear stress distribution (d-σ_{xx}, e-σ_{yy}, f-σ_{xy}) at t=7200s of drying. (T_a = 80˚C,v_a= 1.5 m/s, RH = 20%)

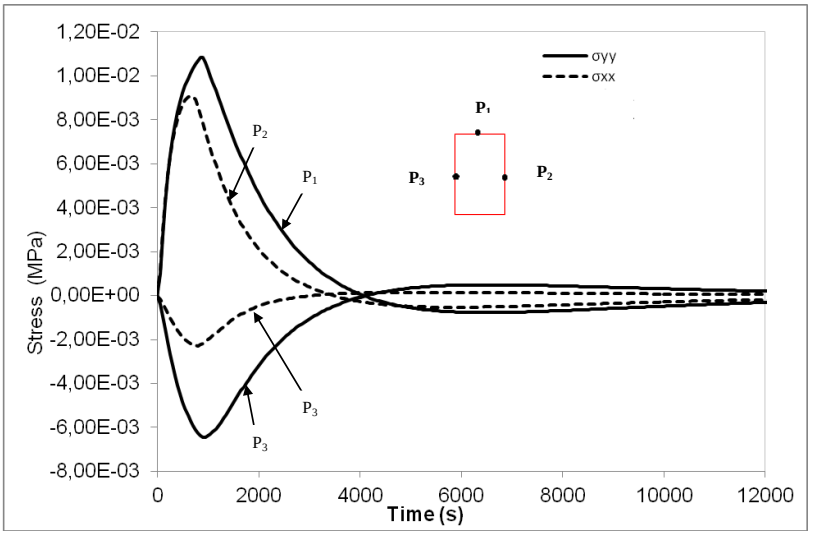

Figure 7: Stress in the x and y directions versus time.

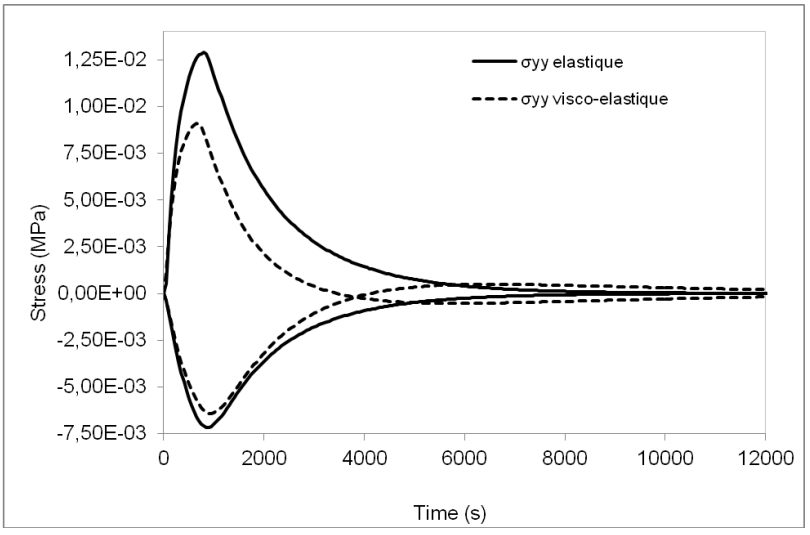

Figure 8: Evolution of stress in the y direction simulated by viscoelastic and elastic models during drying.

As concerns the sample shape evolution during drying, At the beginning of the process, the simulated sample shape showed concave curvatures and at the end of the process, the simulated sample shape turned out to be rectangular and similar to the original one. This result agreed reasonably with the experimental observations. In the case of a long sample of potato with a square section considered as elastic material and dried convectively, Perré and May, (2001) found that the simulated shapes presented slight concave curvatures all over the drying process. However, according to the theoretical results reported by Yang, Sakai, and Watanable (2001) concerning a cylindrical potato sample and admitting an elasto-plastic behavior, the sample shape remained cylindrical and similar to the original one in the first stage of drying while in the second stage of drying the sample shape became convex.

4 Conclusion

An internal drying model coupling heat and mass transport and mechanical behavior witch considered viscoelastic has been developed and numerically implemented with the COMSOL software. It was applied to convective drying of a deformable product saturated with water. The test case was a long parallelepipedical sample of mixture clay dried convectively in a vertical tunnel.

The hydro-thermal part of the model was validated performing experimental measurements in a laboratory hot air dryer. The model was then used to simulate the internal mechanical stresses and the sample shape evolution during drying. A stress reversal phenomenon due to the viscous effect was exhibited. This phenomenon could not be shown when a simpler elastic model was adopted. Besides, a cracking risk in the superficial layer of the sample was demonstrated. The sample shape was also predicted with reasonable accuracy, all over the process.

References

Arrieche, L. S.; Corrêa, R. G.; Sartori, D. J. M. (2009): Drying stresses and strains in a spherical food model. *Computers and Chemical Engineering,* vol. 33, pp. 1805-1813.

Banaszak, J.; Kowalski, S. J. (2005): Theoretical and experimental analysis of stresses and fractures in clay like materials during drying. *Chemical Engineering and Processing,* vol. 44, pp. 497-503.

Chemkhi, S.; Zagrouba, F.; Bellagi, A. (2004): Mathematical model for drying of highly shrinkage media. *Drying Technology,* vol. 22, pp. 1023-1039.

Hammouda, I.; Mihoubi, D. (2013): Modelling of drying induced stress of clay: elastic and viscoelastic behaviours. Mech Time-Depend Mater. *Mechanics of Time-Dependent Materials,* vol. 18, pp. 97-111.

Hassini, L.; Azzouz, S.; Peczalski, R.; Belghith, A. (2007): Estimation of potato moisture diffusivity from convective drying kinetics with correction for shrinkage. *Journal of Food Engineering,* vol. 79, pp. 47-56.

Itaya, Y.; Okouchi, K.; Mori, S. (2001): Effect of heating modes on internal strain-stress formation during drying of molded ceramics. *Drying Technology,* vol. 19, pp. 1491-1504.

Jomaa, W.; Puiggali, J. R. (1991): Drying of shrinkage materials: modelling with shrinkage velocity. *Drying Technology,* vol. 9, pp. 1271-1293.

Kaur, L.; Singh, N.; Sodhi, N. S.; Gujral, H. S. (2002): Some properties of potatoes and their starches. I. Cooking, textural and rheological properties of potatoes. *Food Chemistry,* vol. 79, pp. 177-181.

Khalfaoui, K.; Chemkhi, S.; Zagrouba, F. (2013): Modeling and stress analysis during drying of a deformable and saturated porous medium. *Drying Technology,* vol. 31, pp. 1124-1137.

Kowalski, S. J. (2010): Control of mechanical processes in drying. Theory and experiment. *Chemical Engineering science,* vol. 65, pp. 890-899.

Kowalski, S. J.; Rajewska, K. (2002): Drying-induced stresses in elastic and visco-elastic saturated materials. *Chemical Engineering Science,* vol. 57, pp. 3883-3892.

Kowalski, S. J.; Rajewska, K.; Rybicki, A. (2005): Stresses generated during convective and microwave drying. *Drying Technology,* vol. 23, pp. 1875-1893

Lecomte-Nana, G. L.; Barre, O.; Nony, C.; Lecomte, G.;Terracol, T. (2013): Innovative clay-cellulosic biosourced composite: Formulation and processing. *Ceramic Engineering and Science Proceedings,* vol. 33, pp. 219-232.

Mercier, F. (1996): Séchage de gel d'alumine: Maîtrise de la texture de supports de catalyseurs. *Thèse, Université de Bordeaux I.*

Musielak, G. (2001): Possibility of clay damage during drying. *Drying Technology,* vol. 19, pp. 645-1659.

Peczalski, R.; Falgon, D.; Julien, A.; Boyer, J.C. Vidal-Sallé, E. (2005): Impact of density gradients on the stress level within a green ceramic compact during drying. *Drying Technology,* vol. 23, pp. 71-82.

Perré, P.; May, B. K. (2001): A mathematical drying model that account for the coupling between transfers and solid mechanics. Case of highly deformable products. *Drying Technology,* vol. 19, pp. 1629-1643.

Perré, P.; Passard, J. (2004): A physical and mathematical model able to predict the stress field in wood over a wide range of drying conditions. *Drying Technology,* vol. 22, pp. 27-34.

Qian, L.; Dong, L.; Wang, L. J.; Özkan, N.; Mao, Z. H. (2010): Dynamic viscoelastic properties of sweet potato studied by dynamic mechanical analyzer. *Carbohydrate Polymers,* vol. 79,pp. 520-525.

Rémond, R.; Passard, J.; Perré, P. (2007): The effect of temperature and moisture content on the mechanical behaviour of wood: a comprehensive model applied to drying and bending. *European Journal of Mechanics,* vol. 26, pp. 558-572.

Solomon, W. K.; Jindal, V. K. (2007): Modeling changes in rheological properties of potatoes during storage under constant and variable conditions. *LWT*, vol. 40, pp. 170-178.

Toujani, M.; Djebali, R.; Hassini, L.; Azzouz, S.; Belghith, A. (2014): Hydro-thermo-viscoelastic Based Finite Element Modeling of Apple Convective Drying Process. *CMES,* vol. 98, no. 5, pp. 469-485.

Yang, H.; Sakai, N.; Watanable, M. (2001): Drying Model with non-isotropic shrinkage deformation undergoing simultaneous heat and mass transfer. *Drying Technology,* vol. 19, pp. 441-1460.